Cancer Cell
Article

Induction of Abnormal Proliferation by Nonmyelinating Schwann Cells Triggers Neurofibroma Formation

Huarui Zheng,[1,5] Lou Chang,[1,5] Neha Patel,[1,2] Jiong Yang,[1] Lori Lowe,[3] Dennis K. Burns,[4] and Yuan Zhu[1,*]
[1]Division of Molecular Medicine and Genetics, Departments of Internal Medicine and Cell and Developmental Biology
[2]Department of Pediatrics and Communicable Diseases
[3]Departments of Dermatology and Pathology
University of Michigan Medical School, Ann Arbor, MI 48109, USA
[4]Department of Pathology, University of Texas Southwestern Medical Center, Dallas, TX 75390, USA
[5]These authors contributed equally to this work.
*Correspondence: yuanzhu@umich.edu
DOI 10.1016/j.ccr.2008.01.002

SUMMARY

Recent evidence suggests that alterations in the self-renewal program of stem/progenitor cells can cause tumorigenesis. By utilizing genetically engineered mouse models of neurofibromatosis type 1 (NF1), we demonstrated that plexiform neurofibroma, the only benign peripheral nerve sheath tumor with potential for malignant transformation, results from *Nf1* deficiency in fetal stem/progenitor cells of peripheral nerves. Surprisingly, this did not cause hyperproliferation or tumorigenesis in early postnatal period. Instead, peripheral nerve development appeared largely normal in the absence of *Nf1* except for abnormal Remak bundles, the nonmyelinated axon-Schwann cell unit, identified in postnatal mutant nerves. Subsequent degeneration of abnormal Remak bundles was accompanied by initial expansion of nonmyelinating Schwann cells. We suggest abnormally differentiated Remak bundles as a cell of origin for plexiform neurofibroma.

INTRODUCTION

The hallmark feature of neurofibromatosis type 1 (NF1) is the development of benign peripheral nerve sheath tumor, termed neurofibroma (Cichowski and Jacks, 2001; Riccardi, 1992; Zhu and Parada, 2002). NF1 is a common inherited neurological disease, affecting 1 in 3500 newborns worldwide. Individuals afflicted with NF1 are predisposed to a wide spectrum of derangements, including tumors in the peripheral and central nervous system (PNS and CNS), myeloid leukemia, hyperpigmentation defects of the skin, bone abnormalities, and learning disabilities. The *NF1* gene encodes a protein product (neurofibromin) composed of 2818 amino acids, which is highly conserved during evolution. Neurofibromin is a functional Ras *G*TPase-*a*ctivating *p*rotein (RasGAP) that negatively regulates Ras signaling by accelerating conversion of activated Ras-GTP to inactive Ras-GDP (Ballester et al., 1990; Xu et al., 1990).

Plexiform neurofibroma is the only neurofibroma subtype that has the potential to undergo malignant transformation and progress to malignant peripheral nerve sheath tumors (MPNSTs). MPNST is the most common malignancy associated with NF1 and is responsible for the majority of mortality observed in human NF1 patients (Korf, 1999; Woodruff, 1999). Microscopically, neurofibromas are heterogeneous proliferations composed of a mixture of cells found in normal peripheral nerves, including Schwann cells, fibroblasts, perineurial-like fibroblasts, axons, and mast cells. Recent studies from human tumors (Rutkowski et al., 2000; Serra et al., 2000; Sheela et al., 1990) and mouse models (Zhu et al., 2002) have established the Schwann cell lineage as the true neoplastic element in

SIGNIFICANCE

Identification of cancer stem cells raises the possibility that human cancers likely arise from the stem or progenitor cells possessing self-renewal capabilities. However, the nature of the cell(s) of origin of central and peripheral nervous system tumors remains largely unknown. The development of plexiform neurofibroma during early childhood raises the possibility that this tumor arises from the transformation of fetal stem/progenitor cells during nerve development. Our study demonstrated that early tumor formation is characterized by an expansion of fully differentiated nonmyelinating Schwann cells in a microenvironment with degeneration of normal nonmyelinated axon/Schwann cell relationships and mast cell infiltration. These observations suggest potential future therapies for preventing neurofibroma formation by stabilizing axon-Schwann cell interactions and reducing mast cell infiltration.

neurofibromas. In a mature peripheral nerve, there are two types of Schwann cells: myelinating and nonmyelinating Schwann cells (Jessen and Mirsky, 2005). Myelinating Schwann cells encircle large-diameter (>1 μm) axons with concentric layers of cell membrane in a 1:1 relationship to form lipid-rich, multilamellar myelin sheaths. Small-diameter axons are embedded within and separated by cytoplasmic processes of nonmyelinating Schwann cells. These Schwann cell/axonal complexes, termed Remak bundles, may contain up to 30 or 40 axons in mature nerves (Taveggia et al., 2005). If a fully differentiated Schwann cell is assumed to be the cell of origin of neurofibromas, it remains to be explained how loss of NF1 function leads to the transformation of axon-bearing differentiated Schwann cells into the axon-free Schwann cells that populate neurofibromas.

Clinical studies indicate that plexiform neurofibromas are often identified during early childhood (Waggoner et al., 2000). It has been suggested that these tumors are congenital lesions that arise from fetal stem or progenitor cells during nerve development (Riccardi, 1992). The development of the Schwann cell lineage is a complex process that includes multiple transition phases from migrating neural crest cells to glial restricted progenitor cells (Schwann cell precursors) to two mature cell types—myelinating and nonmyelinating Schwann cells (see Figure S1 available with this article online) (Jessen and Mirsky, 2005). Although Schwann cell precursors (SCPs) were originally identified and widely viewed as glial restricted progenitors that only give rise to Schwann cells in developing peripheral nerves (Dong et al., 1999; Jessen et al., 1994), more recent evidence suggests that at least some of these cells are multipotent and give rise to both Schwann cells and myofibroblasts during development (Joseph et al., 2004; Morrison et al., 1999). Consequently, these cells were also referred to as neural crest stem cells (NCSCs) (Morrison et al., 1999). In this study, we refer to these stem/progenitor cells as SCP/NCSCs, which function as an intermediate cell type between classic migrating neural crest cells and lineage-committed Schwann cells during nerve development (Jessen and Mirsky, 2005). Since loss of heterozygosity (LOH) or biallelic inactivation of the *NF1* gene is a rate-limiting step for neurofibroma formation (Cichowski et al., 1999; Serra et al., 1997, 2000), the question arises whether the key LOH event must occur in fetal stem/progenitor cells during nerve development to initiate plexiform neurofibroma formation. In spite of the importance of NF1 as a model for understanding tumor suppressor gene function, it remains uncertain which cell type(s) in the neural crest/Schwann cell lineage during development and/or in adulthood is the cellular target for *NF1* mutation and how loss of *NF1* in these cells leads to neurofibroma formation.

RESULTS

Targeting an *Nf1* Mutation into Fetal Stem/Progenitor Cells during Nerve Development

We previously showed that *n*eural *c*rest-specific *Nf1* mutant mice ($Nf1^{NC}$) developed hyperplastic lesions in NC-derived sympathetic ganglia and adrenal medulla and died at birth (Gitler et al., 2003). To circumvent early lethality of the $Nf1^{NC}$ mice, we utilized a previously published Cre transgenic strain under the control of the P0 promoter (*P0A*-cre) (Giovannini et al., 2000), which expresses Cre in significantly fewer cells within the PNS during development. We crossed the P0A-cre transgenic mice to a Rosa26-LacZ Reporter strain (R26R-LacZ) that allows us to examine Cre recombinase activity by expression of the β-galactosidase (β-gal) gene (Soriano, 1999). *P0A*-cre-mediated recombination, revealed by X-gal staining, was first detected in neural crest and its derived tissues in cranial-facial regions at embryonic day 9.5 (E9.5) (Figure S2). However, significant β-gal activity was not detected until E11.5 in the trunk region (Figures S3Aa–S3Ad). At E12.5, when peripheral nerves start to innervate both forelimbs and hindlimbs, intense X-gal staining was detected in these peripheral nerves (arrows, Figures S3Ba–S3Bd). To assess the specificity of *P0A*-cre-mediated recombination, we performed X-gal staining on serial transverse sections prepared from the trunk region of E12.5 *P0A*-cre+/R26R-LacZ double transgenic embryos. As shown in Figure 1, β-gal positive cells are specifically distributed throughout the PNS including developing peripheral nerves (Figures 1A–1L). In peripheral nerves, β-gal positive cells are colocalized with three neural crest/Schwann cell lineage markers: $p75^{NGFR}$ (a marker that is expressed in both migrating neural crest cells and SCP/NCSCs) (Figures 1A–1C), GAP43 (Figures 1D–1F), and BLBP (brain lipid binding protein, also known as BFABP or Fabp7) (Figures 1G–1I). Both GAP43 and BLBP are expressed in SCP/NCSCs, but not in migrating neural crest cells (Jessen and Mirsky, 2005). It is worth noting that unlike GAP43 and BLBP, $p75^{NGFR}$ is not neural-specific, as it is expressed in both developing nerves and adjacent muscle cells (Figures 1B and 1C) (Wheeler et al., 1998). The nonneural expression of $p75^{NGFR}$ was further confirmed by double-labeling of $p75^{NGFR}$ with an axonal marker, Tuj1 (arrows, Figure S4). Furthermore, most of these β-gal-positive cells in sciatic nerves did not express S100, a marker for differentiated Schwann cells (Figures 1J–1L) (Jessen and Mirsky, 2005; Murphy et al., 1996). Of note, peripheral nerve development in the thoracic region occurs earlier than in lumbar region. Consistently, a significant number of S100-positive cells were observed in peripheral nerves in the thoracic region (arrows, Figure S3C). At the lumbar region, the transition from migrating neural crest cells to SCP/NCSCs occurs between E10 and E11 (Britsch et al., 2001). Because E11.5 is the earliest time point that we could detect significant β-gal activity in the trunk, we conclude that the major cell type in the peripheral nerves in the lumbar region including sciatic nerves undergoing P0A-cre-mediated recombination is the SCP/NCSC. To further confirm these results, we performed double immunofluorescence and attempted to colocalize the β-gal protein with $p75^{NGFR}$ (Figures 1M–1O), GAP43 (Figures 1P–1R), BLBP (Figures 1S–1U), and Sox10 (Figures 1V–1X) (a marker that is expressed in both migrating neural crest cells and SCP/NCSCs) (Britsch et al., 2001). Collectively, these double-labeling experiments demonstrated that most, if not all of, the β-gal positive cells expressed all four markers. However, only a subset of $p75^{NGFR}$, GAP43, BLBP, or Sox10 positive cells expressed β-gal protein. To inactivate *Nf1* in SCP/NCSCs during nerve development, we bred *P0A*-cre transgenic mice to the $Nf1^{flox/-}$ mice (Zhu et al., 2001) and subsequently generated *Nf1* mutant mice with genotypes of $Nf1^{flox/-}$;*P0A*-cre+ (hereafter, $Nf1^{P0A}KO$).

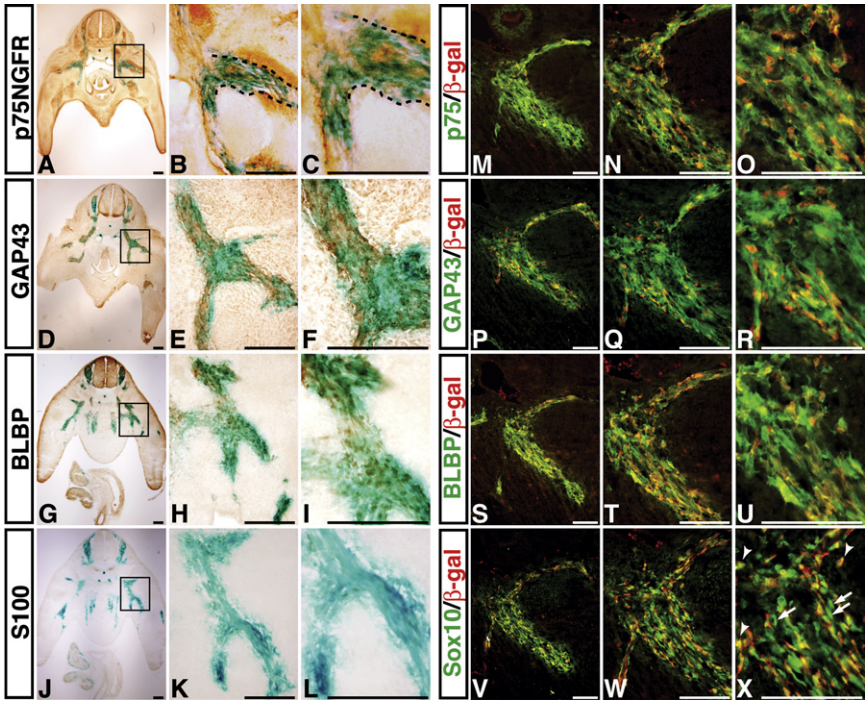

Figure 1. *P0A*-cre-Mediated Recombination in SCP/NCSCs

Transverse sections from the lumbar region of X-gal-stained E12.5 P0A-cre/R26R-LacZ double transgenic embryos were stained with anti-$p75^{NGFR}$ (A–C), GAP43 (D–F), BLBP (G–I), and S100 (J–L) antibodies. The dashed lines (B and C) mark the $p75^{NGFR}$ and β-gal double-positive developing peripheral nerves. The expression of $p75^{NGFR}$ (M–O), GAP43 (P–R), BLBP (S–U), or Sox10 (V–X) in β-gal positive cells was further confirmed by double immuofluorescence. Arrowheads and arrows in X point to Sox10/β-gal double-positive cells and Sox10-positive/β-gal-negative cells, respectively. Scale bars: (A)–(L), 50 μm; (M)–(X), 25 μm.

Loss of *Nf1* in SCP/NCSCs Induces Neurofibroma Formation with High Frequency

The $Nf1^{P0A}$KO mutant mice were viable, fertile, and indistinguishable from their control littermates. However, in the second year of life, all the mutant mice developed signs of sickness including lethargy, ruffled hair, skin lesions, or hindlimb paralysis. Histological analysis revealed that all of the sick mutant mice (n = 14) exhibited neurofibroma formation throughout the PNS. We focused our analysis on sciatic nerves, because these nerves are the only parts of the PNS in which the timing and stages of Schwann cell development are well established (Jessen and Mirsky, 2005). As compared to control nerves (Figures 2A and 2E), all mutant sciatic nerves were significantly enlarged (Figures 2B–2D). Histological examinations of sciatic nerves revealed that 10 of 14 (71%) mutant mice developed full-blown plexiform neurofibromas (NF), which, like human counterparts (Kleihues and Cavenee, 2000), were composed of increased numbers of elongated spindle-shape cells and infiltrating mast cells in a matrix rich in collagen fibers (Figures 2B and 2F and Figures 2C and 2G). All the neurofibromas analyzed in this model expressed S100 and $p75^{NGFR}$ (Figure S5), which often serve as diagnostic markers for human neurofibromas. The neurofibroma tissues were always identified adjacent to preneoplastic lesions (referred to as hyperplasia, Figures 2B and 2C). The major histopathological distinction between hyperplasia and a fully developed neurofibroma is that hyperplasia does not disrupt normal nerve structure in spite of increased cellularity. Figure 2D illustrates an example of advanced hyperplasia, characterized by dramatically increased cellularity with numerous blood vessels (arrowheads) and infiltrating mast cells (arrows), but with persistence of normally arrayed axons. In contrast, a neurofibroma identified in adjacent areas was characterized histologically by complete disruption of nerve structure with only small numbers of residual myelinated nerve fibers (arrows, Figure 2H). In contrast to normal (Figure 2E) and hyperplastic (Figure 2D) nerves in which Schwann cells distribute parallel to nerve fibers, neurofibroma cells are completely disorganized and randomly oriented in a collagen-rich matrix (Figures 2F–2H). The remaining mutant mice without evidence of neurofibroma formation in sciatic nerves (n = 4, 29%) developed an intermediate lesion that we referred to as "hyperplasia with focal neurofibroma" (hyperplasia/NF). Histopathologically, hyperplasia/NF is characterized as an overall hyperplastic lesion with focal areas displaying the disruption of peripheral nerve architecture characteristics of neurofibroma (Figures 7C, 7G, and 7K). Notably, all of these 4 mutant mice also developed large cutaneous or subcutaneous neurofibromas (data not shown), raising the question of whether the presence of these lesions in some way precludes hyperplasia/NF in sciatic nerves from progressing to full-blown neurofibromas. Together, these observations indicate that *Nf1* inactivation in SCP/NCSCs in sciatic nerves induces neurofibroma formation with high frequency.

To test whether differentiated Schwann cells are susceptible to neurofibroma formation, we analyzed sciatic nerves of a previously characterized *Nf1* mutant strain ($Nf1^{flox/-}$;*Krox20*-cre+, referred to as $Nf1^{Krox20}$*KO*) (Zhu et al., 2002). In sciatic nerves, the *Krox20*-cre transgene (also known as Egr2-cre) is first expressed at E15.5 $S100^{+}$ immature Schwann cells at moderate levels. *Krox20*-cre becomes highly expressed during myelination and is maintained in myelinating Schwann cells in adulthood (Figure S1) (Garratt et al., 2000; Ghislain et al., 2002; Voiculescu et al., 2000). None of the sciatic nerves analyzed from 16 aged $Nf1^{Krox20}$*KO* mutant mice along with 3 control littermates (12–16 months old) exhibited any evidence of neurofibroma formation (Figures 2I–2P). In contrast, all of these mutant mice developed multiple neurofibromas in cranial nerves and spinal roots (Zhu et al., 2002) where *Krox20*-cre is expressed in E10.5 neural stem/progenitor cells during early nerve development (Figures S6A–S6C) (Hjerling-Leffler et al., 2005; Maro et al., 2004). The level of *Krox20*-cre-mediated *Nf1* deletion between sciatic nerves and spinal roots was not significantly different (Figure S6D). Furthermore, the level of Cre-mediated recombination in adult sciatic nerves between *P0A*- and *Krox20*-cre transgenic

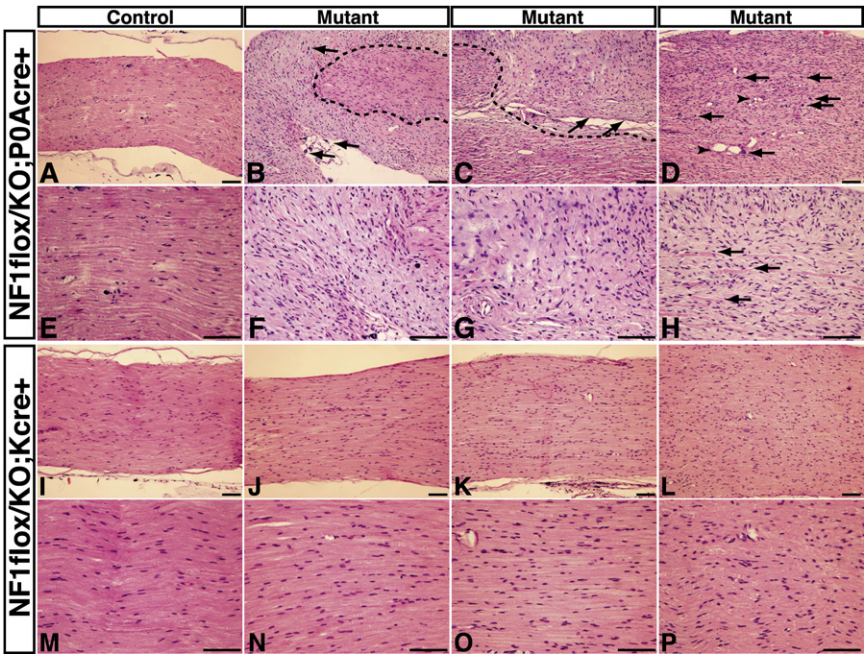

Figure 2. Histological Analysis of Control and Mutant Sciatic Nerves

Sciatic nerves from control (A and E) and three *Nf1*^{P0A}*KO* mice ([B] and [F], [C] and [G], and [D] and [H]) were sectioned and stained with hematoxylin and eosin (H&E). The dashed lines (B and C) mark the border of neurofibromas (arrows, [C]) and hyperplasia in mutant nerves. Arrows in (B) and (D) point to infiltrating mast cells and arrowheads (D) point to blood vessels. Sections from sciatic nerves of control (I and M) and three *Nf1*^{krox20}*KO* ([J] and [N], [K] and [O], and [L] and [P]) mice were stained with H&E. These mutant mice only developed varying degrees of hyperplasia in sciatic nerves. Scale bar, 100 μm.

mice was also not significantly different (Figures S6E and S6F). Therefore, these results suggest that the timing of *Nf1* inactivation, but not the number of *Nf1*-deficient cells generated by *Krox20*- and *P0A*-cre transgenes in peripheral nerves, is critical for the discrepancy in tumor penetrance observed in these two neurofibroma models. Together, these results suggest that in order to efficiently form neurofibromas, *Nf1* must be deleted from fetal stem/progenitor cells (SCP/NCSCs) in developing peripheral nerves.

The Role of *Nf1* in Schwann Cell Development

The genetic studies described above raise the question of whether *Nf1* deficiency leads to the hyperproliferation of fetal stem/progenitor cells (SCP/NCSCs) throughout the late gestation and the early postnatal period, despite the fact that tumors did not become grossly evident until late adulthood. To test this, we examined sciatic nerves of the *Nf1*^{P0A}*KO* mutant mice at postnatal day 22 (P22), a time point when Schwann cell development is nearly complete. Surprisingly, no significant difference in cell density and p75^{NGFR} expression was detected between sciatic nerves of control and mutant mice (Figures 3A–3E). Moreover, ultrastructural analysis obtained with transmission electron microscopy (TEM) revealed no difference in the number of myelinating and nonmyelinating Schwann cells between control and mutant sciatic nerves (Figure S7A). The number of axons within the Remak bundles of mutant sciatic nerves was not significantly altered when compared to the control nerves (Figure 3F, Figure S7B). These observations indicate that *Nf1* does not regulate the generation or overall differentiation of myelinating or nonmyelinating Schwann cells from fetal stem/progenitor cells in developing peripheral nerves. However, unlike control Remak bundles (Figure 3G) in which most of individual axons were segregated into single Schwann cell pockets (Taveggia et al., 2005), some mutant Remak bundles exhibited a Schwann cell "pocket defect" that contained aberrantly large numbers of unseparated axons (Figures 3H, 3I, and 3L), a significant number of which had an abnormal "dilated" morphology in cross sections. The maximum number of axons per pocket in the control nerves was 17 as compared to 41 in the mutant nerves. In addition, some of the abnormal Remak bundles with poorly segregated and dilated axons underwent aberrant myelination (Figure 3K), a phenomenon that was never observed in wild-type nerves (CTR versus Mut, $p = 0.004$). Myelinated Remak bundles with smaller numbers of axons were found in one *Nf1* heterozygous mouse (Figure 3J). Thus, these data suggest that *Nf1* is required for appropriate axonal segregation and suppression of myelination in at least some nonmyelinating Schwann cells.

Degeneration of Abnormal Remak Bundles

To investigate the possible mechanisms by which abnormal Remak bundles lead to neurofibroma formation, we analyzed sciatic nerves of control and *Nf1*^{P0A}*KO* mutant mice at older ages. At 3 months of age (P90), although there was no significant difference in size between control and mutant sciatic nerves, the cellular density of mutant sciatic nerves was significantly increased as compared to that of control nerves (Figures S9A and S9B; Figure 3E). EM analysis indicated that the number of myelinating Schwann cells in mutant P90 sciatic nerves was not significantly different from that of controls (Figures 4A–4C; Figure S7C). Thus, these observations indicate that myelinating Schwann cells do not contribute to initial cellular expansion in P90 mutant nerves. In the nonmyelinating Schwann cell lineage, most of the abnormally differentiated Remak bundles with unseparated or poorly segregated axons observed in P22 mutant sciatic nerves were no longer detected. The small number of such abnormal Remak bundles identified at P90 had "broken" Schwann cell pockets in which axons were dissociating from each other and from their supporting Schwann cells (arrows, Figures 4E and 4F), which was never observed in control Remak bundles (Figure 4D). Since these abnormal Remak bundles typically contained more than 10 axons (10+), we compared the number of axons ensheathed by nonmyelinating Schwann cells within each Remak bundle between control and mutant nerves. Consistent with the degenerating morphology of abnormal Remak

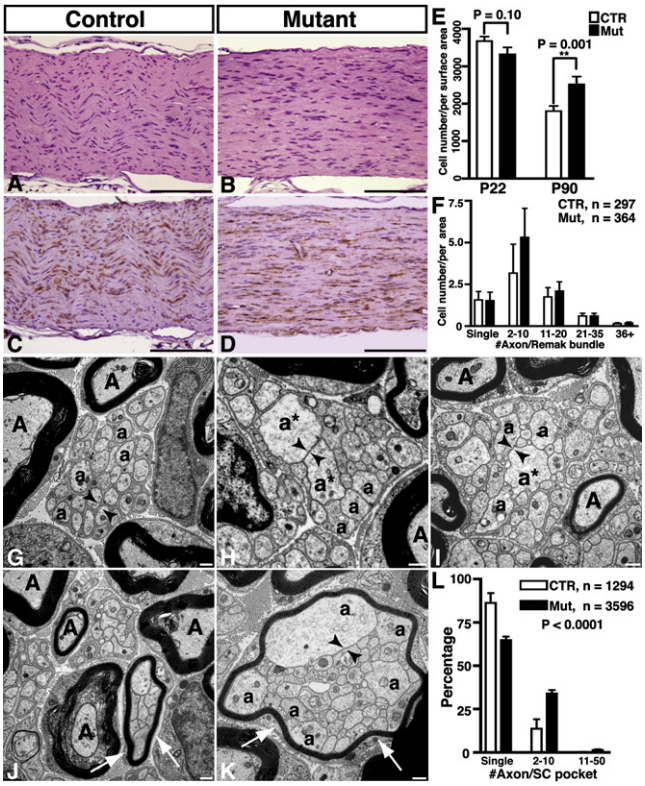

Figure 3. Abnormal Remak Bundles in *Nf1* Mutant Sciatic Nerves

Sections of sciatic nerves from P22 control and $Nf1^{P0A}KO$ mutant mice were stained with H&E (A and B) and anti-$p75^{NGFR}$ antibody (C and D). (E) Quantification of the number of cells per surface area (mm^2) in P22 and P90 control and mutant sciatic nerves. For P22 analysis, 8 control and 3 mutant mice were used, and for P90 analysis, 3 control and 7 mutant mice were used. Cell density for the P22 and P90 is plotted as mean ± SEM. (F) The numbers of Remak bundles per surface area (1,000 μm^2) in control and mutant P22 sciatic nerves were categorized into five groups based upon the number of axons that they ensheathed. N values represent Remak bundles quantified for each genotype. Data in (F) represent mean ± SEM from 2 control and 4 mutant nerves. Transmission electron microscopy (TEM) analysis of Remak bundles in sciatic nerves of P22 control (G and J) and mutant (H, I, and K) mice show abnormal axonal segregation in the mutant mice. Arrowheads in [G] indicate Schwann cell cytoplasm between different axons, which isolates each individual axon into a dedicated Schwann cell pocket in the Remak bundle. Mutant Remak bundles contain unsegregated axons, which remain directly apposed to each other (arrowheads, [H], [I], and [K]). (J and K) The number of myelinated Schwann cells ensheathing multiple axons (arrows) is significantly increased in mutants compared to controls ($p = 0.0036$). (L) The percentage distribution of axons per Schwann cell pocket in control and mutant nerves. N values indicate the number of Schwann cell pockets counted for each genotype (mean ± SEM). The majority of axons in control nerves were segregated into individual pockets, while the number of axons properly segregated was dramatically reduced in mutant nerves (Chi-square goodness-of-fit test, $p < 0.0001$). A, myelinated axons; a, unmyelinated axons; a*, dilated axons. Scale bars: (A)–(D), 100 μm; (G)–(K), 1 μm.

bundles, we found that the normal Remak bundles containing 10+ axons in mutant nerves were dramatically reduced as compared to controls (bottom panel, Figure 4O). Loss of the specific populations of the normal Remak bundles (10+) in P90 mutant nerves suggests that these cells either died or converted to other abnormal cells. To test these two possibilities, we first employed three independent assays to examine whether excess apoptotic cells were present in mutant nerves. No excess apoptotic cells were identified by expression of activated Caspase 3 or by a TUNEL assay in control or mutant sciatic nerves of P22 and P90 mice (Figures S8A–S8H). Furthermore, by using EM, we examined the morphology of over 1,500 nonmyelinating Schwann cells in control and mutant sciatic nerves of P22 and P90 mice. No cell exhibited classic morphology of apoptotic Schwann cells such as coarse chromatin, aggregation in the nucleus, vacuolation in the cytoplasm (Figure S8I) (Feldman et al., 1999). These results indicate that excess apoptosis is not likely to account for the loss of abnormally differentiated Remak bundles observed in mutant nerves.

Next, to test the possibility whether these abnormal Remak bundles converted into other cells, we quantified the number of the different cell types in control and mutant sciatic nerves of P90 mice by EM (Figure S7C). The cells with Schwann cell morphology, defined by presence of a continuous basal lamina and association with axon(s), constitute approximately 98% of the total cells in the endoneurial space in these EM cross sections of both control and mutant nerves. We identified three abnormal Schwann cell populations in mutant nerves that were rarely seen in control nerves (Figures 4D–4O). Abnormal nonmyelinating Schwann cells (anmSCs) were characterized by an association of morphologically abnormal axons (e.g., dilated or naked axons), many of which had myelin-like fragments (Figures 4G–4I). Dissociating Schwann cells (dSCs) were characterized by presence of free Schwann cell processes (arrowheads, Figures 4J and 4K), which progressively dissociated from axons leading to degeneration of unmyelinated axons (arrows, Figures 4K and 4L). Unassociated Schwann cells (uSCs) completely lost axonal contact in spite of presence of a continuous basal lamina that sometimes encircled collagen fibers (Figures 4M and 4N). The uSCs are morphologically identical to the tumor cells observed in both human and mouse neurofibromas (Figure S14) (Cichowski et al., 1999; Lassmann et al., 1977; Zhu et al., 2002). Both anmSCs and dSCs share fundamental features with nonmyelinating Schwann cells: ensheathing small-diameter axon(s) and possessing a continuous basal lamina (Figures 4G–4L). However, most of these abnormal Schwann cells, particularly dSCs, contained fewer numbers of axons (<10) compared to normal nonmyelinating Schwann cells (Figure 4O). Together, these observations suggest that the Remak bundles with large numbers of axons (10+), which were specifically lost in mutant nerves, had broken down into bundles with smaller numbers of axons that were identified within both normal and abnormal (anmSCs and dSCs) Remak bundles. Consistent with this, when we counted and pooled the total axons from all three populations of nonmyelinating Schwann cells in mutant nerves (nmSCs, anmSCs, and dSCs), we found that, as compared to controls, mutant nerves contained significantly fewer Remak bundles ensheathing more than 20 axons, but had increased numbers of Remak bundles containing 10 or fewer axons (Figure S7D). Thus, these results collectively suggest that abnormally differentiated Remak bundles in mutant nerves are unstable and degenerate into anmSCs and dSCs. The presence of anmSCs and dSCs leads to approximately 61% increase ($p < 0.01$) in the number of nonmyelinating Schwann cells in the EM cross sections of P90 mutant nerves as compared to controls

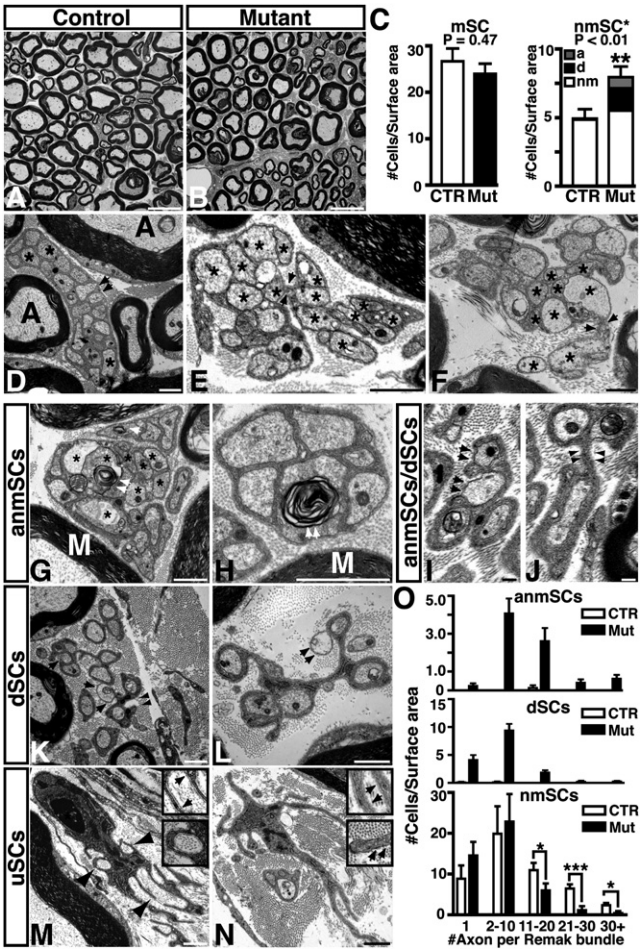

Figure 4. Degeneration of *Nf1* Mutant Remak Bundles at P90

Electron micrographs show cross-sections of P90 control (A and D) and mutant (B, E, and F) sciatic nerves. (C) The number of myelinating (mSC) and nonmyelinating (nmSC) Schwann cells in P90 control and mutant sciatic nerves was presented by the cell number per surface area (mean ± SEM). a, abnormal nmSCs; d, dissociating SCs; nm, normal nmSCs. Arrows in (D) point to a typical Remak bundle in control nerves containing multiple unmyelinated axons (*). (E) and (F) show two examples of abnormally differentiated Remak bundles with "broken pockets" that have dissociating axons. Arrows in (E) and (F) point to unsegregated axons (*) dissociating from each other. (G) and (H) show two representative anmSCs containing "naked" axons and myelin-like fragments (arrows). M, normal myelin. (I) and (J) show the morphological similarity between a pair of anmSC and dSC. Arrows in (I) point to "naked" axons in an anmSC whose degeneration likely generates free Schwann cell processes seen in a dSC (arrowheads, [J]). (K and L) Two examples of dSCs with free Schwann cell processes (arrowheads, [K]) and degenerating unmyelinated axons (arrows). (M and N) Two examples of unassociated Schwann cells (uSCs) with continuous basal lamina and no axon contact. Arrowheads in (M) point to collagen fibers ensheathed by uSCs, which were also shown in Insets (M) with higher magnification. Arrows in the Insets of (M) and (N) (top) point to continuous basal lamina in uSCs as compared to a fibroblast process (arrows, bottom inset in [N]). (O) The numbers of Remak bundles per surface area (1,000 μm^2) in control and mutant sciatic nerves were categorized into five groups based upon the number of axons that they ensheathed. Data in [O] represent mean ± SEM from 2 control and 3 mutant nerves. Top panel, abnormal nonmyelinating Schwann cells (anmSCs); middle panel, dissociating Schwann cells (dSCs); bottom panel, normal nonmyelinating Schwann cells (nmSCs). *$p < 0.05$, ***$p < 0.001$. Scale bar, 1 μm.

(Figure 4C and Figure S7C). uSCs represented a minor population of cells in P90 mutant nerves. Because some of them exhibited only parts of Schwann cell-like processes in the EM images and, hence, are difficult to quantify accurately, we did not include uSCs in this analysis. Therefore, the 61% increase of nonmyelinating Schwann cells observed in P90 mutant nerves most likely is a slight underestimation.

Expansion of Nonmyelinating Schwann Cells

To investigate whether the initial expanded nonmyelinating Schwann cells observed in mutant nerves are neurofibroma cells in the early stages of tumorigenesis, we first attempted to identify specific markers for these cells. Under the light microscope, except for presence of mild hyperplasia, mutant sciatic nerves were relatively normal compared to controls at P90 (Figures 5A and 5B; Figures S9A and S9B). Furthermore, the presence of excess cells in mutant nerves did not alter overall nerve structure and differentiation of myelinating Schwann cells, revealed by S100 staining (Figures S9C and S9D). These observations are consistent with the EM analysis that the myelinating Schwann cells were not affected in these hyperplastic mutant nerves. Since Sox10 is primarily expressed in myelinating Schwann cells of adult nerves (Berger et al., 2006; Peirano et al., 2000), we used Sox10 immunofluorescence to quantify the number of myelinating Schwann cells in control and mutant nerves. Sox10-positive cells (arrowheads) were comparable in control and mutant nerves, whereas mutant nerves had significantly more Sox10-negative cells (arrows, Figures 5C and 5D; Figure S10). These results are consistent with the EM analysis described above (Figure 4C) that the cells in the nonmyelinating, but not in the myelinating, Schwann cell lineage, are expanded in P90 mutant nerves. In addition, these observations also suggest that the initial expanded cellular population in mutant nerves does not resemble fetal stem or progenitor cells with regard to Sox10 expression. To further confirm these results, we employed three additional neural crest/Schwann cell lineage markers, BLBP, GFAP (glial fibrillary acidic protein), and $p75^{NGFR}$. The expression of BLBP is downregulated in mature Schwann cells (Kurtz et al., 1994; Miller et al., 2003). Consistently, no BLBP expression was found in control or mutant sciatic nerves of P90 mice (data not shown). GFAP is probably one of the most reliable markers for nonmyelinating Schwann cells (Jessen and Mirsky, 2005). Accordingly, we observed a conspicuous increase in GFAP-positive cells in mutant nerves as compared to controls (Figures 5E and 5F; Figure S11). Similar to Sox10, $p75^{NGFR}$ is expressed in both migrating neural crest cells and SCP/NCSCs during early nerve development. However, in contrast to Sox10, $p75^{NGFR}$ is only expressed in the nonmyelinating Schwann cell populations in adult nerves. In conjunction with the ultrastructural changes noted above, the expression pattern of Sox10 and BLBP provide compelling evidence that no stem or progenitor cells persisted into adult *Nf1* mutant nerves. Hence, the expression of $p75^{NGFR}$ can be used as a surrogate marker for nonmyelinating Schwann cells in adult mutant nerves. The increased number of $p75^{NGFR}$-expressing cells was identified in mutant nerves compared to controls. These results were demonstrated by two independent assays: immuohistochemistry (Figures 5G and 5H; Figures S9E, S9F, and S12) and flow cytometry (Figures 5I and 5J). Because both GFAP and $p75^{NGFR}$ have diffuse

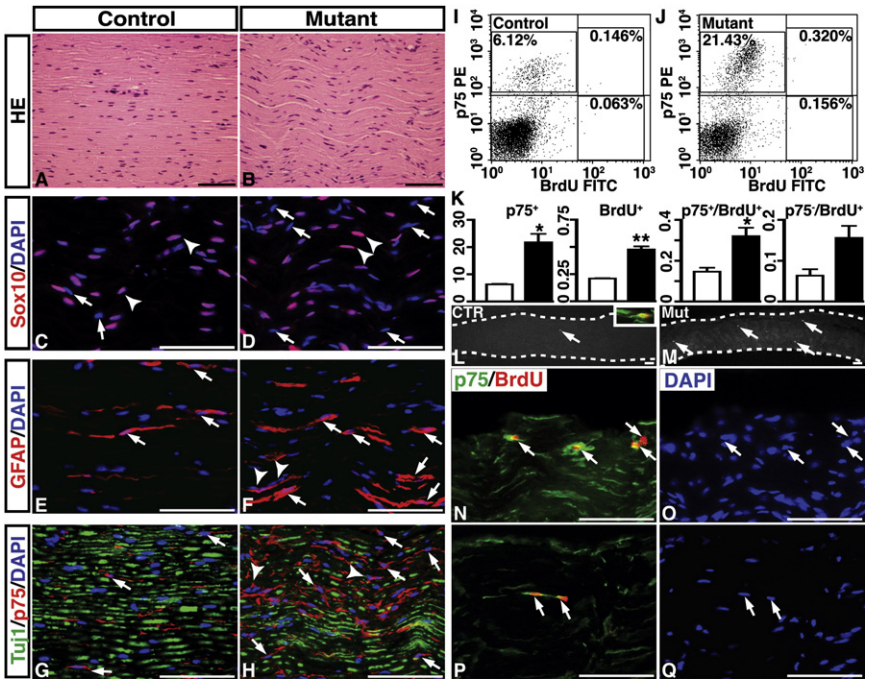

Figure 5. The Expanded Cellular Populations in P90 Mutant Nerves Express Lineage Markers by Nonmyelinating Schwann Cells

Sections from sciatic nerves of P90 control and mutant mice were stained with H&E (A and B), Sox10/DAPI (DAPI stains for cell nuclei) (C and D), GFAP/DAPI (E and F), and Tuj1/p75/DAPI (G and H). Arrows and arrowheads in (C) and (D) point to Sox10-negative and Sox10-positive cells, respectively. The number of GFAP-positive and $p75^{NGFR}$-positive cells was conspicuously increased in mutant nerves (arrows, [F] and [H]) compared to controls (arrows, [E] and [G]). Arrowheads in (F) and (H) point to a cluster of GFAP-positive and $p75^{NGFR}$-positive nuclei in mutant nerves, which were never seen in controls. Representative flow-cytometry plots demonstrate approximately a 2.5-fold increase in frequency of $p75^{NGFR}$-positive cells in mutant nerves (21.75%, [J]) compared to that in control (6.27%, [I]) and a 1.3-fold increase in frequency of BrdU-positive cells in mutant (0.476%, [J]) nerves compared to controls (0.209%, [I]) nerves. Data in (K) represent mean ± SEM from two independent experiments using age-matched control (n = 2) and mutant (n = 4) mice. *$p < 0.05$, **$p < 0.01$. Statistical significance is indicated by * or **. Sections from sciatic nerves of BrdU-treated control (L) and mutant (M) mice were stained with anti-BrdU. The inset in (L) shows a $p75^{NGFR}$/BrdU double-positive cell in a control nerve. ([N] and [O] and [P] and [Q]) Two representative mutant nerves showing a cluster of $p75^{NGFR}$/BrdU double-positive cells (arrows). Scale bar, 50 μm.

expression pattern in the cytoplasm that could not always readily be colocalized with the cell nuclei, we employed flow cytometry to quantify the number of $p75^{NGFR}$-expressing cells in sciatic nerves. In two independent experiments, the frequency of $p75^{NGFR}$-expressing cells isolated by fluorescence-activated cell sorting (FACS) was approximately 2.5-fold higher in mutant nerves than that in controls (Figures 5I–5K), which agreed very well with the increase in Sox10-negative cells (2.1-fold increase; Figure S10K). It is worth noting that the increase observed in the Sox10-negative or $p75^{NGFR}$-positive cell populations of mutant nerves is markedly higher than the increased numbers of non-myelinating Schwann cells obtained from EM analysis (61%). This discrepancy could reflect the fact that we were using longitudinal sections for quantifying Sox10-positive or -negative cells whereas EM images were taken from cross-sections of the nerves. Together, these results demonstrate that the expanded cellular populations in P90 mutant nerves not only morphologically resemble differentiated nonmyelinating Schwann cells at ultrastructural level (e.g., ensheathing small-diameter axons), but also exhibited molecular characteristics that are similar to nonmyelinating Schwann cells ($BLBP^-/Sox10^-/GFAP^+/p75^+$), but not to the fetal stem/progenitor cells ($BLBP^+/Sox10^+/GFAP^-/p75^+$).

The Expanded Nonmyelinating Schwann Cells Exhibit the Characteristics of Early-Stage Neurofibroma Cells

To investigate whether the expanded nonmyelinating Schwann cells in *Nf1* mutant nerves exhibit the characteristics of tumor cells, we examined proliferation of these cells. In normal P90 nerves, only about 0.2% of the total cells were proliferating, revealed by BrdU staining in the FACS plot (Figure 5I). There was nearly 1.3-fold increase in the number of BrdU-positive cells in mutant nerves (Figure 5J) as compared to controls (Figure 5I). Although the number of BrdU-positive cells was increased in both $p75^{NGFR}$-positive and $p75^{NGFR}$-negative cellular compartments, only the $p75^+/BrdU^+$ cells were statistically significant more in mutant nerves than those in control nerves (Figure 5K). To confirm these FACS analyses, we performed BrdU-labeling experiments on the tissue sections from P90 control and mutant sciatic nerves. Consistent with the FACS results, very few BrdU-positive cells could be identified in control nerves, which were evenly distributed throughout the nerve (Figure 5L). In contrast, significantly more BrdU-positive cells were identified in mutant nerves (arrows, Figure 5M; $p = 0.02$). Many of the mutant BrdU-positive cells also expressed $p75^{NGFR}$ and distributed in clusters (Figures 5N–5Q), a characteristic of tumor cells that was never observed in control nerves. Furthermore, a cluster of GFAP or $p75^{NGFR}$-positive nuclei could readily be identified in mutant nerves (arrowheads, Figures 5F and 5H), but not in controls (Figures 5E and 5G).

Both human genetic studies and mouse models have demonstrated that NF1 deficiency and expansion of $NF1^{-/-}$ cells drive neurofibroma formation. If the expanded $p75^{NGFR}$-expressing cells in mutant nerves are early-stage neurofibroma cells, they should be genetically *Nf1* deficient. To mark *Nf1*-deficient cells in intact nerve tissues, we introduced the R26R-LacZ allele to control and mutant mice. Consequently, we could mark $Nf1^{+/-}$ and $Nf1^{-/-}$ cells as β-gal-positive cells in control (*Nf1*$^{flox/+}$;*P0A*-cre+;R26RLacZ) and mutant (*Nf1*$^{flox/-}$;*P0A*-cre+;R26RLacZ) nerves, respectively. As compared to controls (Figure 6A), the number of β-gal-positive cells in mutant (Figure 6B) sciatic nerves were significantly increased, indicating expansion of $Nf1^{-/-}$ cellular compartment. In control nerves (Figure 6C),

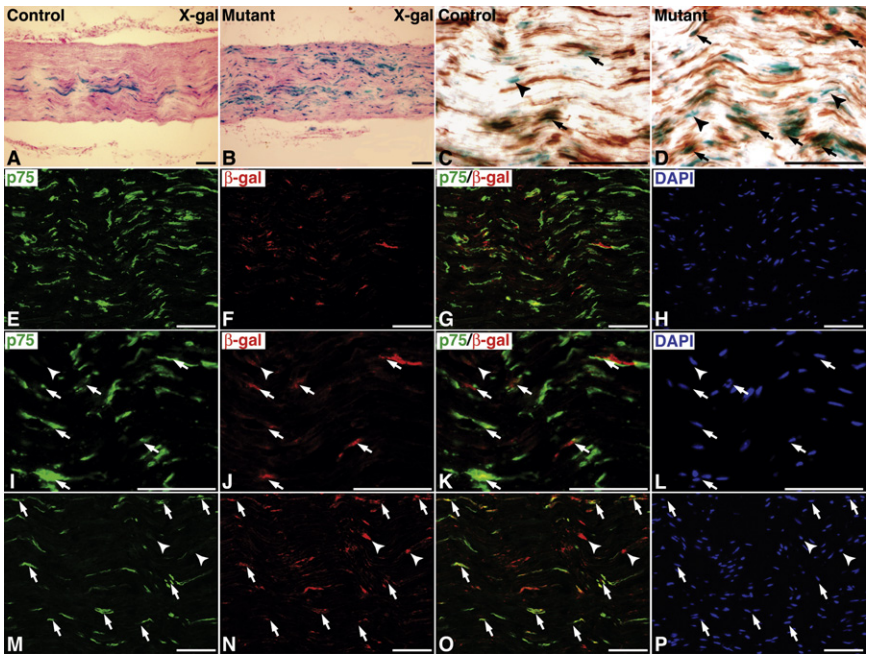

Figure 6. The Expanded *Nf1*-Deficient Cells in P90 Mutant Nerves Express $p75^{NGFR}$ and GFAP

The R26R-LacZ allele was introduced to the control and $Nf1^{P0A}KO$ mutant mice. Sciatic nerves from P90 mice were sectioned and stained with X-gal (A and B) and X-gal/anti-$p75^{NGFR}$ antibody (C and D). Sections from mutant nerves were triple-labeled by anti-$p75^{NGFR}$ (E and I), anti-β-gal (F and J), and DAPI (H and L). Overlay images are shown in (G) and (K). Arrows and an arrowhead in (I) to (L) point to $p75^{NGFR}$/β-gal double-positive cells and a $p75^{NGFR-}$/β-gal+ single positive cell, respectively. Sections from mutant nerves were triple-labeled by anti-GFAP (M), anti-β-gal (N) and DAPI (P). An overlay image is shown in panel (O). Arrows in (M)–(P) point to GFAP/β-gal double positive cells and arrowheads in the same panels show a small number of β-gal positive cells that do not express GFAP. Scale bars, 50 μm.

β-gal-positive cells were found in both $p75^{NGFR}$-positive (arrows) and negative (arrowhead) cell compartments, indicating that P0A-cre was targeted to both nonmyelinating and myelinating Schwann cell lineages. Most of the β-gal positive cells in mutant nerves expressed $p75^{NGFR}$ (Figures 6D and 6E–6L), indicating expansion of the β-gal^{+}/$p75^{NGFR+}$ cellular population. Furthermore, these β-gal positive cells also expressed GFAP (arrows, Figures 6M–6P), further confirming that they are in the nonmyelinating Schwann cell lineage. Together, these results indicate that the expanded nonmyelinating Schwann cells exhibited the key features of neurofibroma cells: increased proliferation, clustering, and most importantly, *Nf1* deficiency. Expansion of the nonmyelinating Schwann cells was accompanied by degeneration of unmyelinated axons, which was revealed by EM analysis (Figures 4K and 4L) and focal loss of Tuj1 expression in mutant nerves (compare Figures S12E and S12M to Figures S12A and S12I). Axonal degeneration also correlated with an inflammatory response. At P22, no mast cells were identified in either control or mutant sciatic nerves. In contrast, mutant nerves recruited over 2.5-fold more mast cells than did controls at P90, a time point when initial cellular expansion was observed in mutant nerves (Figure S13). The degenerative microenvironment and accompanying mast cell infiltration may provide a favorable niche for proliferation of early-stage tumor cells.

Progression Stages of Neurofibroma Development

The morphological, molecular and genetic analyses described above suggest that the expanded $p75^{+}$/$GFAP^{+}$/β-gal^{+} (*Nf1* deficient) nonmyelinating Schwann cells observed in P90 $Nf1^{P0A}KO$ mutant sciatic nerves are tumor cells engaged in the early stages of neurofibroma development. To determine the role of these early-stage tumor cells during tumor progression, we analyzed 6 healthy *Nf1* mutant mice at 6 to 12 months of age, in which we identified the preneoplastic lesions in sciatic nerves similar to those seen in end-stage mutant nerves as described above (Figure 2). These observations suggest that hyperplasia and hyperplasia/NF are the precursors for neurofibroma. However, unlike the hyperplastic lesions observed in sciatic nerves of younger P90 mutant mice (Figure 5B; Figures S9B and S9D), similar lesions in aged mutant nerves exhibited focal loss of myelinated axons, revealed by loss of S100 staining (arrows, Figure 7B) as compared to age-matched controls (Figure 7A). Significantly increased $p75^{NGFR}$ expression also occurred in these mutant nerves (arrows, Figure 7F) compared to controls (Figure 7E), indicating further expansion of these $p75^{NGFR}$-expressing cell populations (compare Figures 7F and 7J to Figures 7E and 7I). In semithin sections, control nerves were tightly packed with myelinated axons with only a small intervening interstitial space (Figures 7M and 7Q). Aged hyperplastic mutant nerves, in contrast, were significantly enlarged by an expanded interstitial compartment (Figures 7N and 7R). The expression pattern of S100 and $p75^{NGFR}$ revealed that hyperplasia/NF (Figures 7C, 7G, and 7K) and neurofibromas (Figures 7D, 7H, and 7L) had continuous expansion of the $p75^{NGFR}$-expressing cells similar to that observed in hyperplasia, leading to further increased interstitial cellularity and depletion of myelinated axons (Figures 7O and 7S, 7P and 7T, and Figure S14). The expanded cell population also expressed GFAP and was *Nf1* deficient, revealed by increased numbers of GFAP-positive (Figures 8A–8I) and R26R-LacZ positive cells (Figure S15) in mutant nerves during tumor progression. Consistent with loss of myelinated axons at later stages of neurofibroma development, gradual loss of Sox10-positive cells was observed in these mutant nerves during tumor progression (Figures 8J–8O). Furthermore, no BLBP expression was observed in these aged mutant nerves (data not shown). Together, these results suggest that neurofibroma progression is driven by continuous expansion of the *Nf1*-deficient cells with molecular characteristics of nonmyelinating Schwann cells ($BLBP^{-}$/$Sox10^{-}$/$GFAP^{+}$/$p75^{+}$) similar to the early-stage tumor cells that were identified in sciatic nerves of younger P90 mutant mice.

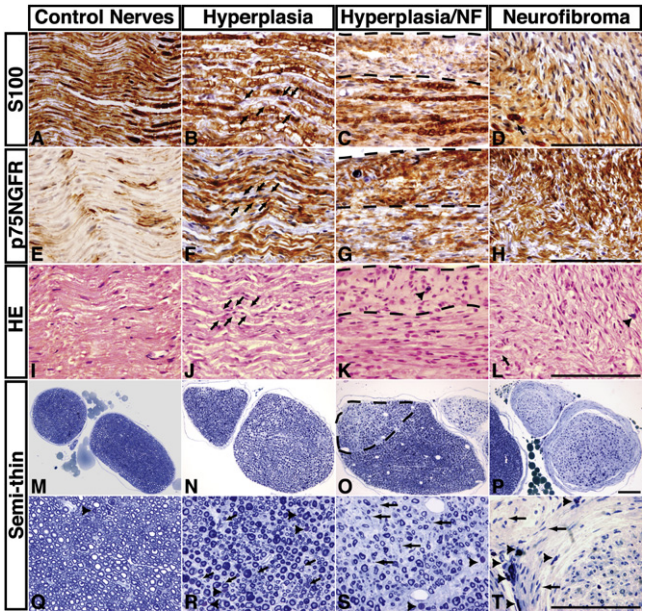

Figure 7. Progression Stages of Neurofibroma Formation

Sciatic nerves from control (A, E, and I) and *Nf1*^{P0A}*KO* mutant mice harboring hyperplasia (B, F, and J), hyperplasia with focal neurofibroma (C, G, and K), and neurofibroma (D, H, and L) were sectioned and stained with anti-S100, anti-p75^{NGFR}, and H&E. Arrows in (B), (F) and (J) point to focal loss of S100-positive myelin sheath that was accompanied by increased numbers of p75^{NGFR}-expressing cells. The dashed lines in (C, G, and K) mark the border of hyperplasia and neurofibroma tissues. Arrows in (D) and (L) point to residual S100-positive myelin sheath in a neurofibroma. Arrowheads in (K) and (L) point to infiltrating mast cells in neurofibroma tissues. Semithin sections of sciatic nerves from control (M and Q) and mutant mice harboring hyperplasia (N and R), hyperplasia with focal NF (O and S), and neurofibroma (P and T) were stained with toluidine blue. The dashed lines in (O) mark the areas undergoing transition from hyperplasia to neurofibroma, which is characterized by significant loss of myelinated axons at ultrastructural levels. Arrows in (R), (S), and (T) point to increased numbers of cells between myelinated axons in mutant nerves compared to controls. Arrowheads (Q–T) point to infiltrating mast cells, staining metachromatically in this preparation. Scale bars, 100 μm.

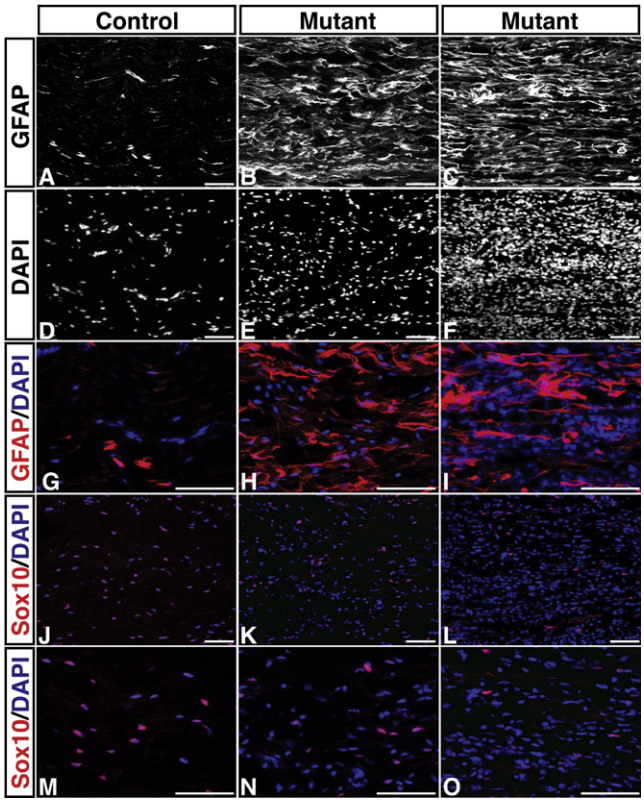

Figure 8. The Number of GFAP-Positive Cells Is Gradually Increased during Neurofibroma Progression with a Concomitant Decrease in Sox10-Expressing Cells

Adjacent sections from sciatic nerves of aged control and two *Nf1*^{P0A}*KO* mutant mice were stained with GFAP (A, B, and C), DAPI (D, E, and F), GFAP/DAPI (overlay images, [G], [H], and [I]), and Sox10/DAPI (J, K, and L). (M), (N), and (O) represent high magnification views of (J), (K), and (L). Scale bars, 50 μm.

DISCUSSION

Cell of Origin for Plexiform Neurofibroma

In this study, we employed two Cre transgenic strains, *P0A*-cre and *Krox20*-cre, which, respectively, target an *Nf1* mutation into stem/progenitor cells and more differentiated Schwann cells in sciatic nerves. The *Nf1*^{P0A}*KO* mice, but not the age-matched *Nf1*^{Krox20}*KO* mice, developed plexiform neurofibromas in sciatic nerves. These genetic studies provide compelling evidence that plexiform neurofibromas arise most efficiently as a result of *Nf1* deletion from fetal stem/progenitor cells in developing peripheral nerves.

No stem/progenitor cells (NCSCs) have been identified in normal adult peripheral nerves (Kruger et al., 2002). Thus, the possible mechanisms underlying transformation of fetal stem/progenitor cells are that NF1 deficiency (1) promotes self-renewal of fetal stem/progenitor cells to form hyperplasia or tumors during or after nerve development is complete and/or (2) inhibits differentiation of the fetal stem/progenitor cells that leads to at least some of these undifferentiated cells persisting into adult nerves and forming tumors at later stages. Our data show that *Nf1*-deficient fetal stem/progenitor cells differentiate according to a normal time course into Schwann cells. In addition, EM analysis and expression of neural crest/Schwann cell lineage markers revealed no evidence of stem/progenitor cells persisting into adult mutant nerves. By employing a well-established neural stem cell assay (Morrison et al., 1999), Joseph et al. found no evidence for the persistence of NCSCs in *Nf1*-deficient nerves based upon functional clonal assays for the presence of self-renewing, multipotent stem cells (Joseph et al., 2008). Together, these data suggest that it is unlikely that persisting *Nf1*-deficient fetal stem/progenitor cells serve as a direct cell of origin for plexiform neurofibroma. Rather, the only subtle phenotypic abnormality identified in postnatal *Nf1*^{P0A}*KO* mutant nerves is the presence of a subset of the Remak bundles with a Schwann cell "pocket defect," which failed to appropriately segregate ensheathed axons. Abnormal axonal segregation phenotypes observed in *Nf1* mutant Remak bundles are reminiscent of those seen in mice with targeted mutations in the type III neuregulin-1 (NRG1) (Taveggia et al., 2005) or β-secretase BACE1 that is normally required for cleaving the type III NRG1 precursor into the functional form (Hu et al., 2006; Willem et al., 2006), suggesting that *NF1* may be an intracellular component of NRG1/ErbB signaling pathway.

Our data indicate that the abnormally differentiated Remak bundles with the "pocket defect" were degenerating in sciatic nerves of P90 *Nf1*^{P0A}*KO* mutant mice. Most strikingly, degeneration of the abnormal Remak bundles was accompanied by initial cellular expansion in *Nf1*^{P0A}*KO* mutant nerves. At the ultrastructural level, the expanded cell populations exhibited an intermediate morphology between fully differentiated nonmyelinating Schwann cells and neurofibroma cells. Thus, the majority of the expanded cells were morphologically characterized as anmSCs or dSCs, both of which displayed the defining features of nonmyelinating Schwann cells (e.g., ensheathing various numbers of small-diameter axons). When we compared the axon number within each Remak bundle between control and mutant nerves, there is a conspicuous shift in axonal distribution from the more Remak bundles ensheathing >20 axons in control nerves to the more Remak bundles with <10 axons in mutant nerves. Thus, the morphological similarities of and the differences in axon number ensheathed by control and mutant nonmyelinating Schwann cells suggest a lineage relationship between the degenerating abnormally differentiated Remak bundles with the "pocket defect" and anmSCs/dSCs/uSCs. Specifically, we propose a model for neurofibroma initiation (Figure S16): degeneration of abnormally differentiated Remak bundles in mutant nerves, which progressively dissociate from axons and breaks into bundles with smaller numbers of axons, a sequence which eventually generates a continuum of abnormal Remak bundles, ranging from anmSC, dSCs to uSCs. The clinical observation that plexiform neurofibroma is almost exclusively found in individuals with *NF1* germline mutations (Halliday et al., 1991; Woodruff, 1999) also supports the notion that *NF1* plays a critical function(s) during early nerve development. Together, our results implicate the abnormally differentiated Remak bundles as a cell of origin for early-stage neurofibroma cells.

Early-Stage Tumor Cells versus Tumor-Initiating Cells

Our morphological and molecular analyses demonstrate that initial hyperplasia observed in P90 *Nf1* mutant nerves is not due to expansion by stem or progenitor cells, but rather by fully differentiated nonmyelinating Schwann cells. To establish a cell or cells as a cell of origin for a tumor, it is necessary to determine whether these cells are responsible for initiation and progression of tumors. The term "tumor-initiating cells" was recently used to describe a subset of human tumor cells that possess stem cell-like properties and are capable of regenerating tumors when transplanted into immunodeficient mice (Al-Hajj et al., 2003; Singh et al., 2004). The "tumor-initiating cells" were often referred to as cancer stem cells. However, these tumor-initiating cells were isolated from end-stage established tumors, which typically have accumulated numerous mutations that support its growth upon xenotransplantation. Therefore, the tumor-initiating cells or cancer stem cells probably have little or no resemblance to the early-stage tumor cells, which harbor fewer mutations and are responsible for initiating tumor formation in primary tumor sites.

Because the early-stage tumor cells typically are present in smaller numbers and have limited tumorigenic capacities, we designed several in vivo assays to determine their tumor cell characteristics. Given that no stem or progenitor cells were observed in adult *Nf1* mutant nerves, we were able to use p75^{NGFR} as a surrogate for the expanded nonmyelinating Schwann cells. First, both our immunofluorescence and FACS data demonstrate that most of the proliferating cells were identified in the p75^{NGFR}-positive cellular compartment, which were significantly increased in *Nf1* mutant nerves. Second, the proliferating p75^{NGFR}-positive cells histopathologically exhibited an important characteristic of tumor cells, namely a tendency to form clusters, a phenomenon that was never observed in control nerves. Third, most importantly, many of the p75^{NGFR}-positive cells are genetically *Nf1* deficient. Finally, during neurofibroma progression, the continuously expanded cellular populations share the molecular and genetic characteristics (BLBP^{-}/Sox10^{-}/GFAP^{+}/p75^{+}/*Nf1*$^{-/-}$) with those early-stage tumor cells. Taken together, our data suggest that the initially expanded nonmyelinating Schwann cells are early-stage tumor cells, which are responsible for both the initiation and progression of plexiform neurofibromas.

Clinical Implication

Previous studies showed that overexpression of epidermal growth factor receptor (EGFR) or dominant negative ErbB4 induced similar hyperplastic lesions to that seen in P90 *Nf1*^{P0A}*KO* mutant nerves (Chen et al., 2003; Ling et al., 2005). However, these transgenic mice did not develop neurofibromas. Therefore, there must be some intrinsic increase of tumorigenic potential in *Nf1*$^{-/-}$ dSCs and uSCs and/or extrinsic field effects of *Nf1*$^{+/-}$ microenvironment. Intriguingly, we detected unmyelinated axonal degeneration and mast cell infiltration at the initiation phase of neurofibroma formation. Joseph et al. transplanted *Nf1*$^{-/-}$ NCSCs into sciatic nerves of adult *Nf1*$^{+/-}$ mice and observed no tumor formation 20 months after injection (Joseph et al., 2008 [this issue of Cancer Cell]). Therefore, it is tempting to speculate that such a degenerative and inflammatory microenvironment could provide a favorable niche for initial proliferation of *Nf1*$^{-/-}$ cells. Thus, the present study suggests potential future therapies for prevention and treatment of neurofibroma by stabilizing axon-Schwann cell interactions and reducing mast cell infiltration.

EXPERIMENTAL PROCEDURES

Control and Conditional Mutant Mice

The control mice used in this study are a pool of phenotypically indistinguishable mice with four genotypes: *Nf1*$^{flox/+}$;*P0A*-cre+, *Nf1*$^{flox/flox}$;*P0A*-cre−, *Nf1*$^{flox/-}$;*P0A*-Cre−, and *Nf1*$^{+/-}$. The mutant mice used were of the genotype, *Nf1*$^{flox/-}$;P0A-cre (mutants). The P0A-cre transgenic strain was initially generated on the FVB background (Giovannini et al., 2000). After five generations of being backcrossed to the 129 Svj background, the P0A-cre transgenic mice were crossed to the *Nf1*$^{flox/-}$ mice that were maintained on the 129 Svj background. Subsequent crosses generated control and mutant mice for analysis. The Rosa26-LacZ allele was maintained on the mixed 129 Svj and C57Bl6 backgrounds. The mutant mice with or without the Rosa26-LacZ allele exhibited similar phenotypes. All mice in this study were cared for according to the guidelines that were approved by the Animal Care and Use Committees of the University of Michigan at Ann Arbor.

Histological, Molecular, FACS, and Statistical Analyses

Detailed descriptions for these experimental procedures are provided in the Supplemental Data.

Supplemental Data

The Supplemental Data include Supplemental Experimental Procedures and 16 supplemental figures and can be found with this article online at http://www.cancercell.org/cgi/content/full/13/2/117/DC1/.

ACKNOWLEDGMENTS

We thank M. Hancock, J. Tomasek, L. Liu, and A. Wang for technical assistance; members of the Zhu lab for support; Dr. N. Joseph for assistance on FACS analysis; Drs. L. Parada and M. Giovannini for providing critical mouse strains and generous support in the early phases of the project; Dr. P. Charnay for *Krox20*-cre mice; S. Meshinchi at the MIL core facility for EM analysis; J. Kazemi at CSCAR for statistical analysis; Dr. N. Heintz for BLBP antibody and Drs. Y. Shen and K. Meiri for GAP-43 antibody; and Drs. E. Fearon, S. Morrison, and S. Weiss for critically reading the manuscript. This work is supported by grants from the American Cancer Society (ACS, no. RSG DDC-110857), the Department of Defense (DOD, NF050041), the Comprehensive Cancer Center and Biological Sciences Scholars Program of the University of Michigan (Y.Z.). Y.Z. is an ACS, GMCR, and BSSP Scholar.

Received: June 4, 2007
Revised: November 12, 2007
Accepted: January 3, 2008
Published: February 4, 2008

REFERENCES

Al-Hajj, M., Wicha, M.S., Benito-Hernandez, A., Morrison, S.J., and Clarke, M.F. (2003). Prospective identification of tumorigenic breast cancer cells. Proc. Natl. Acad. Sci. USA *100*, 3983–3988.

Ballester, R., Marchuk, D., Boguski, M., Saulino, A., Letcher, R., Wigler, M., and Collins, F. (1990). The NF1 locus encodes a protein functionally related to mammalian GAP and yeast IRA proteins. Cell *63*, 851–859.

Berger, P., Niemann, A., and Suter, U. (2006). Schwann cells and the pathogenesis of inherited motor and sensory neuropathies (Charcot-Marie-Tooth disease). Glia *54*, 243–257.

Britsch, S., Goerich, D.E., Riethmacher, D., Peirano, R.I., Rossner, M., Nave, K.A., Birchmeier, C., and Wegner, M. (2001). The transcription factor Sox10 is a key regulator of peripheral glial development. Genes Dev. *15*, 66–78.

Chen, S., Rio, C., Ji, R.R., Dikkes, P., Coggeshall, R.E., Woolf, C.J., and Corfas, G. (2003). Disruption of ErbB receptor signaling in adult non-myelinating Schwann cells causes progressive sensory loss. Nat. Neurosci. *6*, 1186–1193.

Cichowski, K., and Jacks, T. (2001). NF1 tumor suppressor gene function: narrowing the GAP. Cell *104*, 593–604.

Cichowski, K., Shih, T.S., Schmitt, E., Santiago, S., Reilly, K., McLaughlin, M.E., Bronson, R.T., and Jacks, T. (1999). Mouse models of tumor development in neurofibromatosis type 1. Science *286*, 2172–2176.

Dong, Z., Sinanan, A., Parkinson, D., Parmantier, E., Mirsky, R., and Jessen, K.R. (1999). Schwann cell development in embryonic mouse nerves. J. Neurosci. Res. *56*, 334–348.

Feldman, E.L., Russell, J.W., Sullivan, K.A., and Golovoy, D. (1999). New insights into the pathogenesis of diabetic neuropathy. Curr. Opin. Neurol. *12*, 553–563.

Garratt, A.N., Voiculescu, O., Topilko, P., Charnay, P., and Birchmeier, C. (2000). A dual role of erbB2 in myelination and in expansion of the schwann cell precursor pool. J. Cell Biol. *148*, 1035–1046.

Ghislain, J., Desmarquet-Trin-Dinh, C., Jaegle, M., Meijer, D., Charnay, P., and Frain, M. (2002). Characterisation of cis-acting sequences reveals a biphasic, axon-dependent regulation of Krox20 during Schwann cell development. Development *129*, 155–166.

Giovannini, M., Robanus-Maandag, E., van der Valk, M., Niwa-Kawakita, M., Abramowski, V., Goutebroze, L., Woodruff, J.M., Berns, A., and Thomas, G. (2000). Conditional biallelic Nf2 mutation in the mouse promotes manifestations of human neurofibromatosis type 2. Genes Dev. *14*, 1617–1630.

Gitler, A.D., Zhu, Y., Ismat, F.A., Lu, M.M., Yamauchi, Y., Parada, L.F., and Epstein, J.A. (2003). Nf1 has an essential role in endothelial cells. Nat. Genet. *33*, 75–79.

Halliday, A.L., Sobel, R.A., and Martuza, R.L. (1991). Benign spinal nerve sheath tumors: their occurrence sporadically and in neurofibromatosis types 1 and 2. J. Neurosurg. *74*, 248–253.

Hjerling-Leffler, J., Marmigere, F., Heglind, M., Cederberg, A., Koltzenburg, M., Enerback, S., and Ernfors, P. (2005). The boundary cap: a source of neural crest stem cells that generate multiple sensory neuron subtypes. Development *132*, 2623–2632.

Hu, X., Hicks, C.W., He, W., Wong, P., Macklin, W.B., Trapp, B.D., and Yan, R. (2006). Bace1 modulates myelination in the central and peripheral nervous system. Nat. Neurosci. *9*, 1520–1525.

Jessen, K.R., and Mirsky, R. (2005). The origin and development of glial cells in peripheral nerves. Nat. Rev. Neurosci. *6*, 671–682.

Jessen, K.R., Brennan, A., Morgan, L., Mirsky, R., Kent, A., Hashimoto, Y., and Gavrilovic, J. (1994). The Schwann cell precursor and its fate: a study of cell death and differentiation during gliogenesis in rat embryonic nerves. Neuron *12*, 509–527.

Joseph, N.M., Mukouyama, Y.S., Mosher, J.T., Jaegle, M., Crone, S.A., Dormand, E.L., Lee, K.F., Meijer, D., Anderson, D.J., and Morrison, S.J. (2004). Neural crest stem cells undergo multilineage differentiation in developing peripheral nerves to generate endoneurial fibroblasts in addition to Schwann cells. Development *131*, 5599–5612.

Joseph, N.M., Mosher, J.T., Buchstaller, J., Snider, P., McKeever, P.E., Lim, M., Conway, S.J., Parada, L.F., Zhu, Y., and Morrison, S.J. (2008). The loss of Nf1 transiently promotes self-renewal but not tumorigenesis by neural crest stem cells. Cancer Cell *13*, this issue, 129–140.

Kleihues, P., and Cavenee, W.K. (2000). Pathology and Genetics of Tumors of the Nervous System (Lyon, France: iARC Press).

Korf, B.R. (1999). Plexiform neurofibromas. Am. J. Med. Genet. *89*, 31–37.

Kruger, G.M., Mosher, J.T., Bixby, S., Joseph, N., Iwashita, T., and Morrison, S.J. (2002). Neural crest stem cells persist in the adult gut but undergo changes in self-renewal, neuronal subtype potential, and factor responsiveness. Neuron *35*, 657–669.

Kurtz, A., Zimmer, A., Schnutgen, F., Bruning, G., Spener, F., and Muller, T. (1994). The expression pattern of a novel gene encoding brain-fatty acid binding protein correlates with neuronal and glial cell development. Development *120*, 2637–2649.

Lassmann, H., Jurecka, W., Lassmann, G., Gebhart, W., Matras, H., and Watzek, G. (1977). Different types of benign nerve sheath tumors. Light microscopy, electron microscopy and autoradiography. Virchows Arch. *375*, 197–210.

Ling, B.C., Wu, J., Miller, S.J., Monk, K.R., Shamekh, R., Rizvi, T.A., Decourten-Myers, G., Vogel, K.S., DeClue, J.E., and Ratner, N. (2005). Role for the epidermal growth factor receptor in neurofibromatosis-related peripheral nerve tumorigenesis. Cancer Cell *7*, 65–75.

Maro, G.S., Vermeren, M., Voiculescu, O., Melton, L., Cohen, J., Charnay, P., and Topilko, P. (2004). Neural crest boundary cap cells constitute a source of neuronal and glial cells of the PNS. Nat. Neurosci. *7*, 930–938.

Miller, S.J., Li, H., Rizvi, T.A., Huang, Y., Johansson, G., Bowersock, J., Sidani, A., Vitullo, J., Vogel, K., Parysek, L.M., et al. (2003). Brain lipid binding protein in axon-Schwann cell interactions and peripheral nerve tumorigenesis. Mol. Cell. Biol. *23*, 2213–2224.

Morrison, S.J., White, P.M., Zock, C., and Anderson, D.J. (1999). Prospective identification, isolation by flow cytometry, and in vivo self-renewal of multipotent mammalian neural crest stem cells. Cell *96*, 737–749.

Murphy, P., Topilko, P., Schneider-Maunoury, S., Seitanidou, T., Baron-Van Evercooren, A., and Charnay, P. (1996). The regulation of Krox-20 expression reveals important steps in the control of peripheral glial cell development. Development *122*, 2847–2857.

Peirano, R.I., Goerich, D.E., Riethmacher, D., and Wegner, M. (2000). Protein zero gene expression is regulated by the glial transcription factor Sox10. Mol. Cell. Biol. *20*, 3198–3209.

Riccardi, V.M. (1992). Neurofibromatosis: Phenotype, Natural History, and Pathogenesis, Second Edition (Baltimore and London: Johns Hopkins University Press).

Rutkowski, J.L., Wu, K., Gutmann, D.H., Boyer, P.J., and Legius, E. (2000). Genetic and cellular defects contributing to benign tumor formation in neurofibromatosis type 1. Hum. Mol. Genet. *9*, 1059–1066.

Serra, E., Puig, S., Otero, D., Gaona, A., Kruyer, H., Ars, E., Estivill, X., and Lazaro, C. (1997). Confirmation of a double-hit model for the NF1 gene in benign neurofibromas. Am. J. Hum. Genet. *61*, 512–519.

Serra, E., Rosenbaum, T., Winner, U., Aledo, R., Ars, E., Estivill, X., Lenard, H.G., and Lazaro, C. (2000). Schwann cells harbor the somatic NF1 mutation in neurofibromas: evidence of two different Schwann cell subpopulations. Hum. Mol. Genet. *9*, 3055–3064.

Sheela, S., Riccardi, V.M., and Ratner, N. (1990). Angiogenic and invasive properties of neurofibroma Schwann cells. J. Cell Biol. *111*, 645–653.

Singh, S.K., Hawkins, C., Clarke, I.D., Squire, J.A., Bayani, J., Hide, T., Henkelman, R.M., Cusimano, M.D., and Dirks, P.B. (2004). Identification of human brain tumour initiating cells. Nature *432*, 396–401.

Soriano, P. (1999). Generalized lacZ expression with the ROSA26 Cre reporter strain. Nat. Genet. *21*, 70–71.

Taveggia, C., Zanazzi, G., Petrylak, A., Yano, H., Rosenbluth, J., Einheber, S., Xu, X., Esper, R.M., Loeb, J.A., Shrager, P., et al. (2005). Neuregulin-1 type III determines the ensheathment fate of axons. Neuron *47*, 681–694.

Voiculescu, O., Charnay, P., and Schneider-Maunoury, S. (2000). Expression pattern of a Krox-20/Cre knock-in allele in the developing hindbrain, bones, and peripheral nervous system. Genesis *26*, 123–126.

Waggoner, D.J., Towbin, J., Gottesman, G., and Gutmann, D.H. (2000). Clinic-based study of plexiform neurofibromas in neurofibromatosis 1. Am. J. Med. Genet. *92*, 132–135.

Wheeler, E.F., Gong, H., Grimes, R., Benoit, D., and Vazquez, L. (1998). p75NTR and Trk receptors are expressed in reciprocal patterns in a wide variety of non-neural tissues during rat embryonic development, indicating independent receptor functions. J. Comp. Neurol. *391*, 407–428.

Willem, M., Garratt, A.N., Novak, B., Citron, M., Kaufmann, S., Rittger, A., DeStrooper, B., Saftig, P., Birchmeier, C., and Haass, C. (2006). Control of peripheral nerve myelination by the beta-secretase BACE1. Science *314*, 664–666.

Woodruff, J.M. (1999). Pathology of tumors of the peripheral nerve sheath in type 1 neurofibromatosis. Am. J. Med. Genet. *89*, 23–30.

Xu, G.F., Lin, B., Tanaka, K., Dunn, D., Wood, D., Gesteland, R., White, R., Weiss, R., and Tamanoi, F. (1990). The catalytic domain of the neurofibromatosis type 1 gene product stimulates ras GTPase and complements ira mutants of S. cerevisiae. Cell *63*, 835–841.

Zhu, Y., and Parada, L.F. (2002). The molecular and genetic basis of neurological tumours. Nat. Rev. Cancer *2*, 616–626.

Zhu, Y., Romero, M.I., Ghosh, P., Ye, Z., Charnay, P., Rushing, E.J., Marth, J.D., and Parada, L.F. (2001). Ablation of NF1 function in neurons induces abnormal development of cerebral cortex and reactive gliosis in the brain. Genes Dev. *15*, 859–876.

Zhu, Y., Ghosh, P., Charnay, P., Burns, D.K., and Parada, L.F. (2002). Neurofibromas in NF1: Schwann cell origin and role of tumor environment. Science *296*, 920–922.